Proc. Natl. Acad. Sci. USA
Vol. 93, pp. 2545–2550, March 1996
Biochemistry

Molecular mechanism of transmembrane signaling by the aspartate receptor: A model

(bacterial chemotaxis/x-ray crystallography/distance difference matrices/engineered disulfide bonds/histidine kinases)

STEPHEN A. CHERVITZ AND JOSEPH J. FALKE*

Department of Chemistry and Biochemistry, University of Colorado, Boulder, CO 80309-0215

Communicated by Olke C. Uhlenbeck, University of Colorado, Boulder, CO, December 6, 1995 (received for review September 6, 1995)

ABSTRACT **The aspartate receptor of bacterial chemotaxis is representative of a large class of membrane-spanning receptors found in prokaryotic and eukaryotic organisms. These receptors, which regulate histidine kinase pathways and possess two putative transmembrane helices per subunit, appear to control a wide variety of cellular processes. The best characterized subgroup of the two-helix receptor class is the homologous family of chemosensory receptors from *Escherichia coli* and *Salmonella typhimurium*, including the aspartate receptor. This receptor binds aspartate, an attractant, in the periplasmic compartment and undergoes an intramolecular, transmembrane conformational change, thereby modulating the autophosphorylation rate of a bound histidine kinase in the cytoplasm. Here, we analyze recent results from x-ray crystallographic, solution ^{19}F NMR, and engineered disulfide studies probing the aspartate-induced structural change within the periplasmic and transmembrane regions of the receptor. Together, these approaches provide evidence that aspartate binding triggers a "swinging-piston" displacement of the second membrane-spanning helix, which is proposed to communicate the signal across the bilayer.**

Histidine kinase signaling pathways are widespread in prokaryotic and eukaryotic organisms, where they are often regulated by a class of receptors possessing two transmembrane helices per subunit (1–5). These two-helix receptors, including the aspartate receptor of bacterial chemotaxis, appear to utilize the same mechanism of transmembrane signaling. The strongest evidence for a shared signaling mechanism is provided by hybrid receptors containing complementary regions of two-helix receptors from independent pathways. Such hybrid receptors are fully functional (6); for example, fusion of the ligand-binding domain of the aspartate receptor to the signaling region of a different receptor confers aspartate regulation upon the histidine kinase pathway regulated by the latter receptor (7, 8). The aspartate receptor is a suitable system in which to investigate this shared signaling mechanism since its structure is well characterized and its signaling pathway can be reconstituted *in vitro* (9–10).

The domain organization of the aspartate receptor, a 120-kDa dimer of two identical subunits, is schematically summarized in Fig. 1. The periplasmic ligand-binding domain, whose structure has been crystallographically determined (11, 14), is a 36-kDa dimer of symmetric four-helix bundles. Two helices from each bundle continue across the bilayer (15, 16), yielding the extended helices, denoted α1/TM1 and α4/TM2 (Fig. 1). Within the bilayer, the four membrane-spanning helices of the dimer form a compact, 12-kDa transmembrane domain, the packing arrangement of which has been characterized by disulfide-mapping studies (15–20). The two N-terminal, or first, transmembrane helices (α1/TM1 and α1′/TM1′, where the prime distinguishes different subunits) lie in contact near the central C_2 axis of the dimer, where they stabilize the subunit interface through extensive coiled-coil interactions in both the periplasmic and membrane-spanning domains (12, 14–16). The second transmembrane helices (α4/TM2 and α4′/TM2′) couple the periplasmic domain to the 72-kDa cytoplasmic domain, which forms a stable ternary complex with the histidine kinase (CheA) and a coupling protein (CheW) (21, 22).

Previous studies have shown that the transmembrane signal of the aspartate receptor requires no change in its oligomeric structure (23, 24) and appears to involve relative displacement of the second transmembrane helix within one or both subunits (α4/TM2 and α4′/TM2′) (12, 13, 25). A similar picture has emerged for the closely related receptor for ribose and galactose (26–28). A number of structural models have been offered for the transmembrane signal of this receptor family (11, 17, 18, 29–32), but a lack of direct structural and biochemical evidence has prevented resolution of these alternative views.

Recently, however, three independent approaches have begun to provide the evidence needed to develop a molecular picture for the transmembrane signal of the aspartate receptor. Here, we synthesize and extend the analyses of previous x-ray crystallographic (11), solution ^{19}F NMR (25), and disulfide-engineering studies (12, 13) to develop a simple model for the aspartate-induced conformational change within the periplasmic and membrane-spanning domains. First, to locate the aspartate-induced distance changes within the periplasmic ligand-binding domain, distance-difference matrices are generated to compare the known structures of the apo and aspartate-occupied domain. The resulting matrices confirm that aspartate binding triggers significant movement of the second membrane-spanning helix in one of the two subunits. Moreover, the matrix analysis facilitates the optimal superposition of the apo and aspartate-occupied structures, revealing that the aspartate-induced movement is a "swinging-piston" displacement of the second transmembrane helix, fully capable of communicating the aspartate-induced signal across the bilayer. Further evidence for this swinging-piston displacement is provided by a modeling study of recently described "lock-on" and "lock-off" disulfide bonds, which trap the full-length receptor in the kinase-activating and -inactivating states, respectively. Finally, the swinging-piston model is consistent with published ^{19}F NMR results identifying the second membrane-spanning helix as the transmembrane signaling element. Altogether, the results of three independent approaches strongly support the swinging-piston model, providing what may become the first molecular description of a ligand-induced transmembrane conformational change.

METHODS

Distance-Difference Analysis of the Aspartate-Induced Conformational Change. The method of Nishikawa *et al.* (34) was used to generate distance-difference matrices comparing

The publication costs of this article were defrayed in part by page charge payment. This article must therefore be hereby marked "*advertisement*" in accordance with 18 U.S.C. §1734 solely to indicate this fact.

*To whom reprint requests should be addressed.

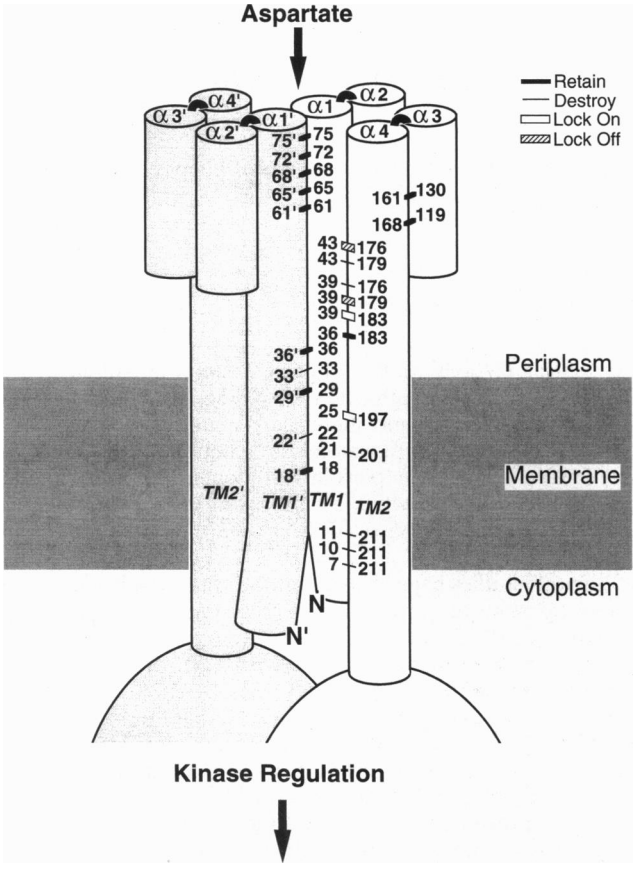

FIG. 1. Schematic structure of the aspartate receptor, summarizing the effects of engineered disulfides on transmembrane-kinase regulation. Shown are the three structural regions of the homodimeric receptor: (*i*) the periplasmic ligand-binding domain (11), (*ii*) the transmembrane region, and (*iii*) the cytoplasmic signaling domain. The indicated 23 disulfide bonds were previously engineered into the periplasmic and transmembrane regions, where they were designed to covalently link the interfaces between adjacent helices (12, 13). These disulfides are divided into three classes by their differing effects on receptor-mediated kinase regulation: one class retains substantial kinase regulation (≥20% native modulation by aspartate), another class essentially destroys kinase regulation (≤10% native modulation by aspartate), and the third class locks the kinase on or off (see text). For simplicity, helix and disulfide perspectives have been altered, and intrasubunit disulfides are shown for only one of the two symmetric subunits.

the apo and aspartate-occupied crystal structures of the *Salmonella typhimurium* ligand-binding domain containing the engineered Cys^{36}—$Cys^{36'}$ disulfide bond (11). These matrices, which summarize the aspartate-induced distance changes within the isolated domain, were generated by computing the α-carbon separations within each crystal structure (residues 32–180 of both subunits), followed by subtraction of the apo distance matrix from the aspartate-occupied distance matrix. Loops α1–α2 and α2–α3, which were perturbed by crystal packing or undefined in at least one crystal structure, were omitted from the analysis (see Fig. 2 legend).

Superposition of the Apo and Aspartate-Occupied Structures. To probe the molecular details of the ligand-induced signal, the apo and aspartate-occupied crystal structures of the Cys^{36}—$Cys^{36'}$ ligand-binding domain (11) were superimposed by Biosym Insight II software, using the static B subunit as a structural reference. Specifically, the superposition targeted residues 44–175 of the B subunits, omitting loops α1–α2 and α2–α3. The validity of this superposition was confirmed by comparing the root mean square deviations (rmsds) of alternative overlays, again omitting loops α1–α2 and α2–α3 (see *Results*).

One alternative superposition, in which the A subunits are overlaid to orient the two dimer conformations, has been shown to yield an apparent 4° rotation of the subunits relative to one another when aspartate binds (refs. 11 and 23 and unpublished data). Such an aspartate-induced, intersubunit movement is disfavored, however, by published ^{19}F NMR and engineered-disulfide results (12, 13, 25) and is directly contradicted by the present distance-difference analysis indicating that large regions of the subunit interface are not perturbed by ligand binding. In contrast, the use of the B subunit to orient the superposition is supported by the same experimental evidence (see *Results*).

The superimposed dimers were used to quantify the aspartate-induced displacements of the four membrane-spanning helices as follows. For each helix, α-carbon displacements were calculated for a 12-residue section of standard helix near the center of its crystallographically determined length. These distances were then averaged to yield the mean translational displacement. Angular displacements were determined from the angle formed between the corresponding helical axes of the superimposed structures. For the α4/TM2 signaling helix, identical estimates of the translational and angular components were provided by the XPLOR software package (35), which was used to carry out a two-step superposition (translation, then rotation) of this helix within the overlaid dimers.

Modeling the Transmembrane Helices. To estimate the helix displacements required to form lock-on and lock-off disulfides, modeling was used to extend the helices of the ligand-binding domain into the predicted bilayer region. The analysis focused on the two transmembrane helices of subunit A: α1/TM1 and α4/TM2, respectively. (*i*) To extend the α1/TM1 helix into the bilayer, the coiled-coil α1/TM1 helix modeled by Scott and Stoddard (17), representing residues 1–36 of subunit A, was utilized. The backbone atoms of residues 32–36 within this helix were superimposed onto the corresponding atoms of helix α1 in the apo crystallographic dimer (11), yielding the full transmembrane helix α1/TM1. (*ii*) To extend the α4/TM2 helix, a canonical right-handed α-helix representing residues 170–213 was built. Then, the backbone atoms of residues 170–176 were superimposed on the corresponding atoms of the crystallographic α4/TM2 helix.

RESULTS

Aspartate-Induced Distance Changes in the Ligand-Binding Domain. The known crystal structures (11) of the apo and aspartate-occupied ligand-binding domains were compared by distance-difference analysis (34) to identify, in a model-independent way, the structural elements displaced by aspartate binding to the isolated periplasmic fragment. Both crystal structures included the engineered Cys^{36}—$Cys^{36'}$ intersubunit disulfide bond (20), which stabilized the homodimeric domain for crystallization (11). The same disulfide has been shown to retain native kinase regulation when incorporated into the full-length receptor (12), while the isolated domain containing this disulfide exhibits an aspartate affinity indistinguishable from that of the wild-type receptor in its native membrane (25, 36). It follows that the Cys^{36}—$Cys^{36'}$ disulfide stabilizes the native structure and function of the ligand-binding domain, thereby minimizing the perturbations observed when the isolated domain lacks such a crosslink (36).

The method of Nishikawa *et al.* (34) was used to generate distance-difference matrices in which the two subunits of the ligand-binding domain are labeled A and B, respectively. Briefly, interatomic distances within the aspartate-occupied structure were calculated for (*i*) all pairs of α-carbons in different subunits and (*ii*) all pairs of α-carbons in the same subunit. From these distances, the corresponding interatomic distances within the apo structure were subtracted, yielding the

aspartate-induced distance change for each α-carbon pair. These distance changes are plotted in Fig. 2 *A* and *B* as inter- and intrasubunit distance-difference matrices, respectively, highlighting the ligand-generated perturbations of magnitude exceeding 0.5 Å.

The resulting distance-difference matrices reveal a large, aspartate-induced displacement of helix α4/TM2 within subunit A, which is known to make most of the contacts with the bound aspartate molecule (11). Upon aspartate binding, the α4/TM2 helix is observed to move at least 1 Å with respect to each helix of the other subunit (Fig. 2*A*) and also is displaced 1 Å relative to helix α1/TM1 of the same subunit (Fig. 2*B*). Somewhat smaller aspartate-induced displacements are also observed for helix α3 of subunit A and for the loops or helix termini in the vicinity of the aspartate-binding site (Figs. 2 *A* and *B*). However, no concerted helix displacements are observed either at the subunit interface (Fig. 2*A*) or within the B subunit (Fig. 2*B*). Thus, unlike the α4/TM2 helix of the A subunit, the remaining three membrane-spanning helices of the dimer remain relatively stationary upon aspartate binding.

Superposition of the Apo and Aspartate-Occupied Structures. To generate a molecular picture of the ligand-induced conformational change, the apo and aspartate-occupied structures (11) of the ligand-binding domain were superimposed. The distance-difference matrices greatly facilitated this superposition by demonstrating the static nature of the B subunit (Fig. 2*B*), whose structure is relatively independent of ligand binding. Thus, the apo and aspartate-occupied dimers were

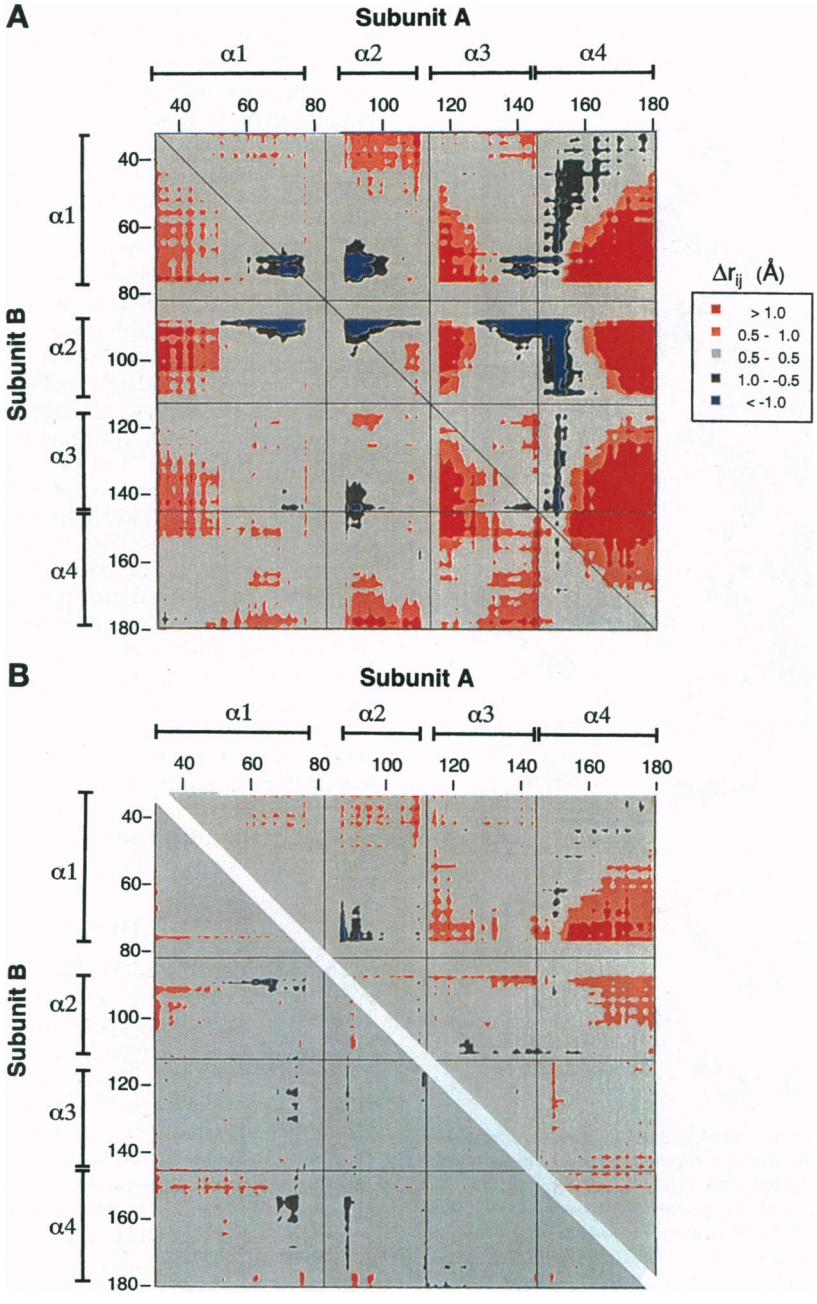

FIG. 2. Distance-difference matrices showing aspartate-induced distance changes in the periplasmic ligand-binding domain. Colors indicate the aspartate-induced distance changes (r_{ij}, Å) between pairs of α-carbons in the ligand-binding domain, calculated by using the apo and aspartate-occupied crystal structures (11). (*A*) Intersubunit distance changes. (*B*) Intrasubunit distance changes within subunit A (upper right) or subunit B (lower left). The axes specify the residue numbers within each subunit, as well as the positions of the periplasmic helices. No distance changes were calculated for two loops, one of which was undetermined in the aspartate-occupied structure (loop α1–α2, residues M^{76}–T^{87}), while the other was perturbed by crystal packing (loop α2–α3, residues N^{109}–M^{116}).

superimposed by overlaying their B subunits. The validity of this approach was confirmed by a comparison of alternative superpositions: the rmsd observed for superposition of the B subunits alone (0.35 Å) was significantly smaller than that of either the A subunits alone (0.57 Å) or the full A + B dimers (0.77 Å), indicating that the B subunit is indeed the most static structural unit suitable for referencing overlays.

Fig. 3 depicts the resulting superimposed dimers, focusing on the periplasmic regions of the four membrane-spanning helices. As observed in the distance-difference matrices, aspartate binding repositions the α4/TM2 helix within subunit A, while the α1/TM1 helix and the α1′/TM1′ and α4′/TM2′ helices of subunit B are relatively stationary. The displacement consists of a 1.6 ± 0.2 Å downward shift of the α4/TM2 helix toward the cytoplasm, coupled to a 5° tilt of the helix axis, as detailed in the Fig. 3 legend. This two-component helix motion can be termed the swinging piston since it would cause the attached cytoplasmic domain to execute both a pendulum-like swinging movement approximately parallel to the plane of the membrane and a piston-like plunging movement normal to the plane of the membrane (assuming rigid attachment; see below). Similar helix displacements are common features of allosteric proteins, and relative helix movements of ≈1.5 Å typically do not require significant rearrangements of side-chain packing at the helix–helix interface (33, 37). The piston component of the motion is reminiscent of a model proposed by Lynch and Koshland (30), which also predicts a piston motion of ≈1.5 Å but in the opposite direction.

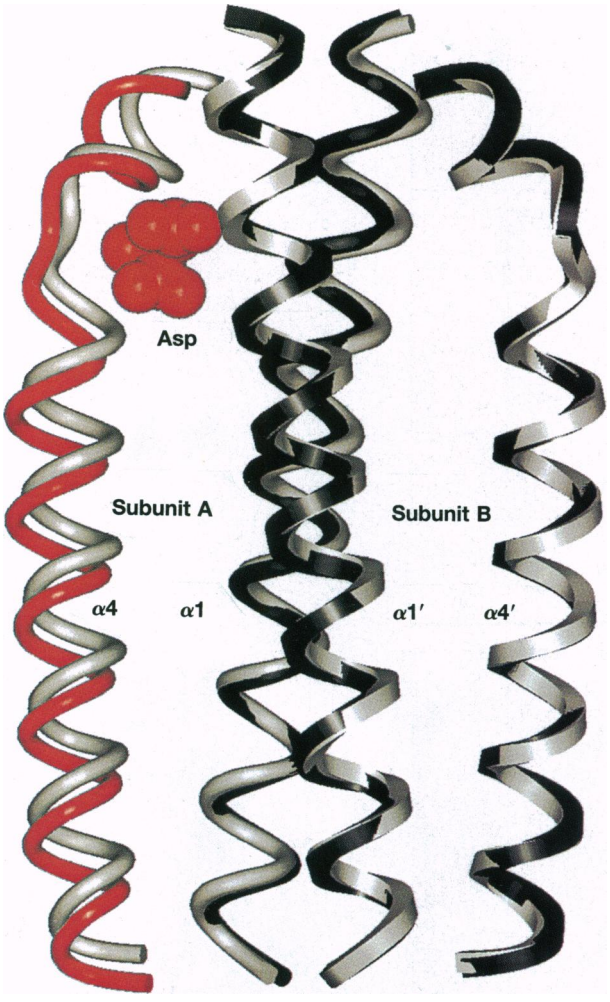

FIG. 3. Aspartate-induced conformational change in the periplasmic ligand-binding domain. Shown is a superposition of the crystal structures (11) for the apo (grey) and aspartate-occupied (black) ligand-binding domain, depicting the single bound aspartate molecule and the periplasmic regions of the four membrane-spanning helices (residues 44–75 of helices α1/TM1 and α1′/TM1′; residues 146–175 of helices α4/TM2 and α4′/TM2′). Upon aspartate binding, the α4/TM2 helix of subunit A is observed to translate 1.6 ± 0.2 Å downward (or toward the cytoplasm in the intact receptor) and to tilt 5°, yielding the new position highlighted in red. By contrast, the remaining three transmembrane helices of subunits A (cylindrical ribbon) and B (square ribbon) are relatively stationary, exhibiting aspartate-induced translational and angular displacements less than 0.5 Å and 1° in magnitude, respectively.

Modeling the Helix Displacements Required to Form Lock-On and Lock-Off Disulfide Bonds. Independent information regarding the nature of the aspartate-induced transmembrane signal was obtained by analyzing the structural change needed to form lock-on and lock-off disulfide bonds. Such engineered disulfides, which covalently link the α1/TM1 and α4/TM2 helices within each monomer, were recently shown to lock the signaling state of the intact, membrane-bound receptor in the kinase-activating or -inactivating modes, respectively. Two lock-off disulfides and one lock-on disulfide are located within the periplasmic region of the α1/TM1-α4/TM2 interface, while the other lock-on disulfide is found in the bilayer region (12, 13).

To investigate the helix displacements trapped by these lock-on and lock-off disulfides, modeling was used to extend the α1/TM1 and α4/TM2 helices into the bilayer. Focusing on the A subunit of the apo dimer, α1/TM1 was extended as a coiled-coil helix paired with α1′/TM1′ (17), while α4/TM2 was modeled as a standard α-helix. Fig. 4 presents the resulting transmembrane helices, including the β-carbons of the lock-inducing cysteine pairs in their reduced state. Interestingly, formation of the Cys^{39}—Cys^{179} and Cys^{43}—Cys^{176} lock-off disulfides would appear to generate a downward piston displacement of the α4/TM2 helix relative to α1/TM1, while the Cys^{39}—Cys^{183} and Cys^{25}—Cys^{197} lock-on disulfides appear to trap an upward piston movement of α4/TM2. Both the magnitude (≈1 Å) and direction of these piston motions are the same as those triggered by ligand binding in the superposition analysis (Fig. 3). Unfortunately, it is difficult to ascertain whether the disulfide-induced displacements include a swinging component since the angular positions of the modeled cysteine pairs are critically dependent on both (*i*) the assumed degree of supercoiling and (*ii*) the precise coupling of the modeled helices to their crystallographic counterparts (Fig. 4, legend). Overall, however, the modeling analysis of lock-on and lock-off disulfides provides strong evidence supporting the piston component of the swinging-piston model.

DISCUSSION

The Swinging-Piston Model. Taken together, the available evidence supports a swinging-piston mechanism for the transmembrane signal of the aspartate receptor, in which the signal is transmitted by a ligand-induced movement of a single transmembrane helix, located within the subunit providing most of the contacts to the bound aspartate molecule. This aspartate-induced displacement of the α4/TM2 signaling helix in subunit A is postulated to involve both a translational piston component and a rotational swinging component, which serve to alter the structure or dynamics of the cytoplasmic signaling domain directly coupled to the C-terminal end of the α4/TM2 helix. The altered cytoplasmic domain, in turn, modulates the activity of its associated histidine kinase protein.

Summary of New and Existing Evidence for the Swinging-Piston Mechanism. The most direct evidence for the proposed α4/TM2 helix displacement is provided by the apo and aspartate-occupied crystal structures of the isolated ligand-binding domain (11). The present comparison of these structures reveals a 1.6 ± 0.2 Å piston translation of α4/TM2 in subunit

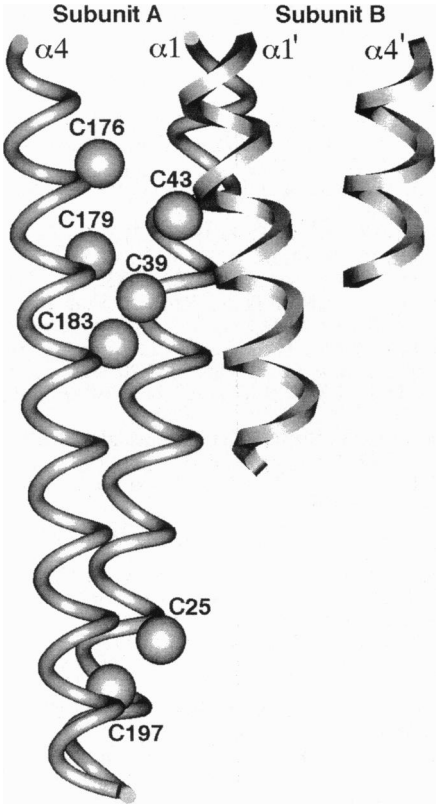

FIG. 4. Relative positions of engineered cysteines yielding lock-on and lock-off disulfide bonds. Shown are the membrane-spanning helices of subunit A (cylindrical ribbon), where the crystallographically determined (11) regions have been extended into the bilayer region by modeling. For comparison, only the crystallographically determined regions of the corresponding helices are illustrated for the B subunit (square ribbon). van der Waals surfaces (spheres) indicate the β-carbons of engineered cysteine pairs which yield lock-on and lock-off disulfide bonds (13): C^{39}, C^{183} (disulfide yields lock on); C^{25}, C^{197} (disulfide yields lock on); C^{43}, C^{176} (disulfide yields lock off); and C^{39}, C^{179} (disulfide yields lock off). The illustrated regions are residues 18–50 and 170–201 of the modeled α1/TM1 (17) and α4/TM2 helices in subunit A, respectively, and residues 32′–50′ and 170′–180′ of the crystallographic α1′/TM1′ and α4′/TM2′ helices in subunit B.

A, as well as a 5° swinging rotation (Fig. 3). These amplitudes are derived from the superimposed structures of the apo and aspartate-occupied dimers, in which the relatively static structure of the B subunit is used to orient the superposition. More generally, the observed displacement of the α4/TM2 signaling helix is an inherent feature of the crystal structure data, since the model-independent distance difference analysis reveals the same aspartate-induced movement of the α4/TM2 helix (Fig. 2). In contrast, the majority of the subunit interface, as well as the three other transmembrane helices of the dimer, is observed to be static in both the distance-difference and superposition analyses (Figs. 2 and 3).

The effects of engineered disulfides on receptor signaling corroborate the aspartate-induced displacement of the signaling helix, indicating that this displacement is not an artifact of domain isolation or crystal packing. Recent studies have placed unique disulfide bonds into the full-length, membrane-bound aspartate receptor, then examined the effect of each disulfide on transmembrane kinase regulation *in vitro* (12, 13). Three inter-helix interfaces were targeted for covalent crosslinking by this approach, as summarized in Fig. 1. (*i*) At the dimer interface, most disulfides (8 of 10) engineered into the contacts between the α1/TM1 and α1′/TM1′ helices were observed to retain substantial transmembrane-kinase regulation, exhibiting 20–100% of the native kinase activation and aspartate regulation. It follows that the transmembrane signal does not require a concerted rearrangement of the subunit interface, a point reinforced by the present distance difference and superposition analyses (Figs. 2*A* and 3). (*ii*) Similarly, at the interface between the α3 and α4/TM2 helices within the same subunit, both disulfides tested were observed to retain substantial kinase regulation, yielding at least 30% of the native kinase activation and aspartate regulation. (*iii*) By contrast, at the interface between the helices α1/TM1 and α4/TM2 in the same subunit, nearly all the engineered disulfides tested (10 of 11) essentially destroyed kinase regulation, allowing no more than 10% of the native aspartate modulation. Furthermore, of these 10 inhibitory disulfides linking the α4/TM2 helix to α1/TM1, 4 were observed to lock the receptor in the on or off signaling states, thereby constitutively activating or inactivating the histidine kinase and decreasing or increasing ligand binding affinity, respectively. Such results directly demonstrate the involvement of α4/TM2 in signaling.

Structural analysis of the engineered lock-on and lock-off disulfides provides further support for the piston component of the swinging-piston mechanism. In the present study, the modeled structures of the α1/TM1 and α4/TM2 transmembrane helices suggest that such disulfides would generate piston-type displacements of the signaling helix, possessing directions and magnitudes similar to those observed in the crystal structure analysis. For example, lock-on disulfide formation is predicted to trap a downward piston motion of α4/TM2 relative to α1/TM1, while lock-off disulfides and aspartate binding are predicted to trigger an upward displacement of α4/TM2. The specific assumptions and potential errors of this modeling analysis prevent the estimation of angular helix displacements, thereby precluding an independent test of swinging movements. However, within these limitations, the known lock-on and lock-off disulfides are fully consistent with the swinging-piston model.

The swinging-piston mechanism also accounts for the conformational changes detected in solution by ^{19}F NMR studies of the isolated ligand-binding domain (25). These studies monitored the ^{19}F chemical shifts of fluorine probes incorporated into intrinsic phenylalanine rings. Significant aspartate-induced chemical shift changes were observed for each of the two probes located on the α4/TM2 helix (F^{150}, F^{180}), while the chemical shifts of the two probes on the α1/TM1 helix (F^{30}, F^{40}) were unaffected by aspartate. It was concluded that the α4/TM2 helix moves upon aspartate binding, while the α1/TM1 helix at the subunit interface is largely static (25). This solution NMR picture is quite similar to that deduced from the crystal structures of the same fragment (Figs. 2 and 3).

Implications for Kinase Regulation. Ultimately the swinging-piston displacement of the α4/TM2 helix in the ligand-binding domain must trigger a structural change within the cytoplasmic domain, which in turn would modulate the kinase activity of the receptor-kinase complex. Such transmembrane regulation could be dominated by either the angular or translational component of the swinging piston. The magnitudes of the two motional components can be directly compared at the location where the α4/TM2 transmembrane helix is expected to enter the cytoplasm (R^{213}), as follows. Assuming that the α4/TM2 helix is rigid and unhindered by the bilayer, it follows that a 5° rotation of the helix about an axis near residue 168 would generate a 5.8-Å translation of its cytoplasmic end, yielding an amplitude 3.6-fold larger than the observed piston component. Despite their different amplitudes, however, either or both components of the swinging-piston displacement could be required for signaling.

In summary, the swinging-piston model is supported by extensive, independent evidence provided by the isolated ligand-binding domain in crystals and solution and the full-length receptor in its native bilayer. Although it is clear that the swinging-piston movement of the second transmembrane helix

is likely to alter the structure or dynamics of the receptor-kinase interaction, it remains to be determined how the cytoplasmic domain translates this displacement into modulation of histidine kinase activity.

We thank Dr. Craig Kundrot for helpful advice, Drs. Craig Kundrot and Arthur Pardi for critically reading the manuscript, Drs. Sung-Hou Kim and Daniel Koshland Jr. for crystallographic coordinates and helpful discussions, Drs. John S. Parkinson and Jeffry Stock for strains and plasmids, Drs. Barry Stoddard and William Scott for model coordinates, and the National Institutes of Health for funding (Grant GM40731 to J.J.F.).

1. Stock, J. B. & Surette, M. G. (1996) *Escherichia coli and Salmonella typhimurium* (Am. Soc. Microbiol., Washington, DC), in press.
2. Alex, L. A. & Simon, M. I. (1994) *Trends Genet.* **10,** 133–138.
3. Swanson, R. V., Alex, L. A. & Simon, M. I. (1994) *Trends Biochem. Sci.* **19,** 485–490.
4. Parkinson, J. S. (1993) *Cell* **73,** 857–871.
5. Hazelbauer, G. L. (1992) *Curr. Opin. Struct. Biol.* **2,** 505–510.
6. Baumgartner, J. W., Kim, C., Brissette, R. E., Inouye, M., Park, C. & Hazelbauer, G. L. (1994) *J. Bacteriol.* **176,** 1157–1163.
7. Utsumi, R., Brissette, R. E., Rampersaud, A., Forst, S. A., Oosawa, K. & Inouye, M. (1989) *Science* **245,** 1246–1249.
8. Krikos, A., Conley, M. P., Boyd, A., Berg, H. C. & Simon, M. I. (1985) *Proc. Natl. Acad. Sci. USA* **82,** 1326–1330.
9. Ninfa, E. G., Stock, A., Mowbray, S. & Stock, J. (1991) *J. Biol. Chem.* **266,** 9764–9770.
10. Borkovich, K. A., Kaplan, N., Hess, J. F. & Simon, M. I. (1989) *Proc. Natl. Acad. Sci. USA* **86,** 1208–1212.
11. Milburn, M. V., Prive, G. G., Milligan, D. L., Scott, W. G., Yeh, J., Jancarik, J., Koshland, D. E., Jr., & Kim, S. H. (1991) *Science* **254,** 1342–1347.
12. Chervitz, S. A., Lin, C. M. & Falke, J. J. (1995) *Biochemistry* **34,** 9722–9733.
13. Chervitz, S. A. & Falke, J. J. (1995) *J. Biol. Chem.* **270,** 24043–24053.
14. Scott, W. G., Milligan, D. L., Milburn, M. V., Prive, G. G., Yeh, J., Koshland, D. E., Jr., & Kim, S. H. (1993) *J. Mol. Biol.* **232,** 555–573.
15. Falke, J. J., Dernburg, A. F., Sternberg, D. A., Zalkin, N., Milligan, D. L. & Koshland, D. E., Jr. (1988) *J. Biol. Chem.* **263,** 14850–14858.
16. Pakula, A. A. & Simon, M. I. (1992) *Proc. Natl. Acad. Sci. USA* **89,** 4144–4148.
17. Scott, W. G. & Stoddard, B. L. (1994) *Structure* **2,** 877–887.
18. Stoddard, B. L., Bui, J. D. & Koshland, D. E., Jr. (1992) *Biochemistry* **31,** 11978–11983.
19. Lynch, B. A. & Koshland, D. E., Jr. (1991) *Proc. Natl. Acad. Sci. USA* **88,** 10402–10406.
20. Falke, J. J. & Koshland, D. E. Jr. (1987) *Science* **237,** 1596–1600.
21. Schuster, S. C., Swanson, R. V., Alex, L. A., Bourret, R. B. & Simon, M. I. (1993) *Nature (London)* **365,** 343–347.
22. Gegner, J. A., Graham, D. R., Roth, A. F. & Dahlquist, F. W. (1992) *Cell* **70,** 975–982.
23. Yeh, J. I., Biemann, H. P., Pandit, J., Koshland, D. E. & Kim, S. H. (1993) *J. Biol. Chem.* **268,** 9787–9792.
24. Milligan, D. L. & Koshland, D. E., Jr. (1988) *J. Biol. Chem.* **263,** 6268–6275.
25. Danielson, M. A., Biemann, H. P., Koshland, D. E., Jr., & Falke, J. J. (1994) *Biochemistry* **33,** 6100–6109.
26. Lee, G. F., Dutton, D. P. & Hazelbauer, G. L. (1995) *Proc. Natl. Acad. Sci. USA* **92,** 5416–5420.
27. Lee, G. F., Lebert, M. E., Lilly, A. A. & Hazelbauer, G. L. (1995) *Proc. Natl. Acad. Sci. USA* **92,** 3391–3395.
28. Lee, G. F., Burrows, G. G., Lebert, M. R., Dutton, D. P. & Hazelbauer, G. L. (1994) *J. Biol. Chem.* **269,** 29920–29927.
29. Kim, S. H. (1994) *Protein Sci.* **3,** 159–165.
30. Lynch, B. A. & Koshland, D. E., Jr. (1992) *FEBS Lett.* **307,** 3–9.
31. Milligan, D. L. & Koshland, D. E., Jr. (1991) *Science* **254,** 1651–1654.
32. Stock, J. B., Lukat, G. S. & Stock, A. M. (1991) *Annu. Rev. Biophys. Biophys. Chem.* **20,** 109–136.
33. Chothia, C. & Lesk, A. M. (1985) *Trends Biochem. Sci.* **10,** 116–118.
34. Nishikawa, K., Ooi, T., Isogai, Y. & Saito, N. (1972) *J. Phys. Soc. Jpn.* **32,** 1331–1337.
35. Brünger, A. T. (1992) XPLOR 3.1, *A System for Crystallography and NMR* (Yale Univ. Press, New Haven, CT).
36. Milligan, D. L. & Koshland, D. E., Jr. (1993) *J. Biol. Chem.* **268,** 19991–19997.
37. Gerstein, M., Lesk, A. M. & Chothia, C. (1994) *Biochemistry* **33,** 6739–6749.